Supporting Information

Christen et al. 10.1073/pnas.1000846107

SI Materials and Methods

Process Flow. The process flow for the localization network screen is diagrammed in Fig. S1 and explained in the following sections.

Construction of the Triply Fluorescently Labeled Reporter Strain and Complementing Plasmids. Seven hundred bas pairs of the 3′ region of *divJ* fused to *mCherry* was PCR amplified with primers 111 and 113 (see primer list below) from pGB211. Primers 110 and 114 were used to amplify a 700 bp fragment downstream of *divJ* from genomic *C. crescentus* DNA. Both PCR products were spliced together by a SOE PCR, cloned into pCR2.1 (TopoTA; Invitrogen) and further subcloned into the suicide vector pNPTS138 via SpeI and EcoRI to produce pNPTS::*divJ*3′::*mcherry*::*divJ*dw. A cassette carrying 700 bp from the 3′ region of *cpaD* and a *yfp* gene translationally fused to a 700 bp long 5′ fragment of *cpaE* was amplified from pHPV227 (1) with primers 80 and 26, cloned into pCR2.1, and subcloned into pNPTS128 via SphI and SpeI to produce plasmid pNPTS138::*cpaD3′*::*yfp*::*cpaE5*'. The *cfp* derivative *mCYPet* was PCR amplified from pET15b::*mCYPet* (2) using primers 81, 72 and cloned into the BamHI, EcoRV sites of plasmid pNPTS138::*cpaD3′*::*yfp*::*cpaE5*' to yield pNPTS128::*cpaD3′*::*mCyPet*::*cpaE5′*. Primers pairs 77, 71 and 73, 76 were used to amplify a 500 bp fragments of the downstream region of *pleC* and a 500 bp region covering the 3′ part of *pleC* from genomic *C. crescentus* DNA. Both PCR products were spliced together by a consecutive SOE PCR step, cloned into pCR2.1 and were further subcloned into pNPTS138 via SpeI and EcoRI to produce pNPTS138::*pleC*SOE. The *yfp* derivative *mYPet* was PCR amplified from pET15b::*mYPet* (2) using primers 75, 74 and cloned into the BamHI and KpnI site of pNPTS138::*pleC*SOE to generate pNPTS::*pleC3′*::*mYPet*::*pleC*dw. The chromosomal copy of *divJ*, *pleC*, and *cpaE* were replaced over three consecutive double homologous recombination steps using plasmids pNPTS::*divJ3′*::*mcherry*::*divJ*dw, pNPTS::*pleC3*'::*mYPet*::*pleC*dw and pNPTS128::*cpaD3′*::*mCyPet*::*cpaE5′*. To generate plasmids used for complementation studies full-length *tacA*, *spmX*, and *cpaE* were PCR amplified using primer 94, 95, primer 104, 105, and primer 78, 79. PCR products were digested with NdeI and NheI or NdeI and SpeI and cloned into the NdeI and NheI sites of the replicating plasmids pBVMCS_6 or pBXMCS_6 (3).

Construction of the *Tn5* Transposon Derivatives *Tn5Pvan* and *Tn5Pxyl*. Primers 65, 85 (see primer list below) were used to PCR amplify the *Tn5* transposase together with an adjacent ampicillin resistance marker from the plasmid pIT2 (4). Primer 65 introduced an NdeI site and the *Tn5* I-end. Primer 85 introduced a SacI site, the *Tn5* O-end, and a synthetic oligonucleotide linker with a primer binding sites for primer 68. The PCR product was cloned into pCR2.1 and further subcloned into pVMCS2 or pXMCS2 (3) via NdeI, SacI to give pVMCS2*::Tn5Pvan* and pVXMCS2*::Tn5Pxyl*, respectively. The transposon derivatives *Tn5Pvan* and *Tn5Pxyl* can be used to fuse any gene to the xylose or vanillate inducible promoters by random *Tn5* transposition. The *Tn5* elements carry at one end a ribosomal binding site, a start codon, and either an outward-facing *Pxyl* or *Pvan* promoter that will allow conditional expression of distal genes (Fig. S2). At the other end of the *Tn5Pvan or Tn5Pxyl* elements, we have introduced an oligonucleotide linker containing binding sites for two nested primers especially designed for semiarbitrary PCR based high throughput mapping of transposon insertion sites.

Transposon Mutagenesis. The *Tn5Pvan* and *Tn5Pxyl* transposon derivatives were delivered into the triply fluorescently labeled *C. crescentus* reporter strain from an *Escherichia coli* S17-1 donor strains harboring either the suicide plasmid pVMCS2*::Tn5Pvan* or pVXMCS2*::Tn5Pxyl* via conjugation. Transposition events were selected onto PYE plates containing Kanamycin (20 μg/mL) and Nalidixic acid (20 μg/mL).

Automated Colony Picking and Prescreening Using a Soft Agar Assay. Individual transposon mutants were arrayed by a CP-7200 colony-picking robot (Norgren Systems) into 96-well plates and grown over night in PYE media containing Xylose (0.1%) or Vanillic acid (500 μM) on an orbital shaker (Labnet). With a custom made 384 floating pin tool (Fig. S5), the mutant library was replica printed onto Q-trays screening plates (Genetix) containing PYE soft agar (0.3% Agar) with and without inducer. After incubation for 3 days, the plates were scanned on a flatbed scanner to digitize the colony images. Images from plates grown with and without inducer were digitally superimposed to detect differential growth (Fig. S5). The sizes of the colonies were automatically measured and a selection was made corresponding to the size of the colony or the differential growth under +/− inducer. Colonies were kept for further study if the absolute size asymmetry +/− inducer was greater than 0.2, or if the normalized colony size (as determined by comparing the colony to 22 neighboring colonies and averaging over +/− inducer) was less than 84% of the average colony size. Thresholds were determined by creating a histogram of colony counts versus thresholds. Thresholds were adjusted to include only the non-Gaussian tail regions of the colony size distributions.

Transposon Insertion Site Mapping by Nested Semi-Arbitrary PCR. Transposon junctions were amplified by a nested semiarbitrary PCR approach using primer pairs 11, 25 and 13, 68. PCR products were treated with ExoI and SAP (NEB) before sequencing using primer 68. The transposon insertion sites were mapped to the *C. crescentus* chromosome using a Perl script described below. All PCR reactions were performed in 96-well format on a DNA Engine Tetrad Thermal Cycler (MJ Research) using BioMix Red (Bioline). First and second round PCRs were cycled with the following programs adding 1 μl of a stationary culture or 1 μl of the first round product directly to the PCR mixture.

First round PCR. (*i*) 94 °C for 3 min, (*ii*) 94 °C for 30 s, (*iii*) 42 °C for 30 s, slope −1 °C per cycle, (*iv*) 72 °C for 1 min, (*v*) go to step *ii*, 6 times, (*vi*) 94 °C for 30 s, (*vii*) 58 °C for 30 s, (*viii*) 72 °C for 1 min, (*ix*) go to step *vi*, 25 times, (*x*) 72 °C for 3 min, (*xi*) 4 °C hold.

Second round PCR. (*i*) 94 °C for 3 min, (*ii*) 94 °C for 30 s, (*iii*) 64 °C for 30 s, (*iv*) 72 °C for 1 min, (*v*) go to step *ii*, 30 times, (*vi*) 72 °C for 3 min, (*vii*) 4 °C hold.

Primer list.

11 GGCCACGCGTCGACTAGTACNNNNNNNNNNACGCC
13 GGCCACGCGTCGACTAGTAC
25 TGTAAAACGACGGCCAGTG
26 CACAGGAAACAGCTATGACC
65 CATATGGGAGATCTGATCAAGAGACAGGTCGACCGATCCCGTACACAAGTAGC
68 GCGTCACACTCATCGGTTGGGTG
71 CTCGCCGGTACCTTTGGATCCGGCCGCCACGAAGTCGCGAGTGATCTT
72 CGGATATCTTTGTACAGTTCGTCCATGCCGT

73 GCGGCCGGATCCAAAGGTACCGGCGAGACCTTC-CCTGGGGCGGCCTTG
74 GGTACCCTACTTATAGAGCTCGTTCATGCCCTC
75 GGATCCGTGAGCAAAGGCGAAGAGCT
76 GAATTCCGGCCTCGCACAGCAGCATC
77 ACTAGTGAGTCGATGCATCTCGAAGAC
78 CATATGCGGCCGACCGACAACGATCCC
79 GCTAGCCTACTTCTTCTTGAACAGGCCCGAG
80 AAACGCATGCCCGACGAGATCCTGCTGAAGCCG-CACG
81 ATGGGATCCGTGAGCAAGGGAGAGGAACTGTTCG
85 AGAGCTCGCGTCACACTCATCGGTTGGGTGACAC-TCTTTCCCTACACGACGCTCTTCCGATCTACTTGTG-TATAAGAGTCAGTTACC
94 AAACATATGACCAAAACGGTCCTTGTCGTC
95 TTTGCTAGCTTCAGCCCGCTTCCTTCATGTCGAC
108 AAACCCCATATGAAACCGCGTCATCAGGTCTCCC
109 TTTACTAGTCTACTCTTCGTCGCTCACATC
110 ATGGACGAGCTGTACAAGTAAGGATCCGGCGC-TCTGGTCTTACCGCAG
111 AAACTAGTCCGCTACGCCGAGTACGCTGA
113 CTGCGGTAAGACCAGAGCGCCGGATCCTTACTT-GTACAGCTCGTCCAT
114 AAAGAATTCCCACCGAACTGCAGGTCG

Sequence Mapping. Automated base pair accurate mapping onto the *Caulobacter* genome was attempted for each *Tn5* insertion using the Perl-script "map.pl." For each *Tn5* insertion sequencing reaction, the map.pl script locates then end of the *Tn5* sequence and starting with the next base pair in the sequencing reaction (the first originating from the *Caulobacter* genome), advances through the sequencing reaction, extending a perfect match within the *Caulobacter* genome, until a single unambiguous match has been made. To check for consistency, the sequences immediately following this unambiguous match within the sequencing reaction and within the *Caulobacter* genome are then compared. If no unambiguous match can be made, or the sequencing reaction is not consistent with the *Caulobacter* genome, the base pair accurate mapping routine has failed. This failure is often due to noisy sequences, single base pair sequencing errors, insertions in duplicated genome regions, or to the annealing of arbitrary primers only a few base pairs away from the *Tn5* insertion site. If the base pair accurate mapping routine fails, attempts are made to map the *Tn5* insertion on the *Caulobacter* genome using the perl-script "mapwithblast.pl" and the associated python-script "NA1000blast.py". Briefly, for each *Tn5* insertion sequencing reaction, the "mapwithblast.pl" script locates the end of the *Tn5* sequence and uses blastn (5) to find the best alignment of the remainder of the sequencing reaction with the *Caulobacter* genome. For expectation scores of the resulting alignment that are better than a user-defined threshold, the *Tn5*-proximal boundary of the resulting alignment is a reasonable estimate (accurate to within tens of base pairs) of the actual *Tn5* insertion site.

Automated Fluorescence Microscopy. Microscopy based screening was performed using a DM6000B automated microscope equipped with a 100 × 1.46 NA HCX Plan APO oil immersion objective (Leica) and a C9100 EM cooled CCD camera (Hamamatsu). The fluorescent channels were excited with a Leica EL6000 metal halide light source coupled via a liquid light guide. Phase contrast images were taken to facilitate automated focusing during data acquisition and were also used in the automated analysis for membrane boundary determination. Three fluorescence channels were imaged, CFP (Ex 438/24 nm, Em 483/32 nm), YFP (Ex 500/24 nm, Em 542/27 nm), and mCHERRY (Ex 562/40 nm, Em 624/40 nm). Phase contrast and fluorescent images were taken at 40 and 100 ms exposure times, respectively. Camera gain was set to zero for phase contrast and 100 for fluorescent channels. Control of the microscope, stages, auto-focusing, camera, and data acquisition was accomplished via a custom software program, KAMS-acquire, developed by one of the authors (Fig. S4). To image mutant strains, live cells were transferred from 96-well growth plates to 48 isolated sample gel pads (1% agarose, 7 mm in diameter, and 0.7 mm thick) on a 100 × 73 × 1.1 mm glass plate (Fig. S3). The microscopy plate was then covered by an oversize (84 × 66 mm) coverslip and sealed with thermoplastic glue before being mounted on the 3-axis stage. The scope was automated for XYZ motion as well as fine focus using a piezo-electric PIFOC PZ 187E Objective Scanner System (Physik Instrumente). Each of the 48 gel pads on a microscopy plate contained a unique mutant strain or a control wild-type strain. Microscopy plates were scanned in an eight column by six row pattern, with wild-type controls at positions (1, 16, 17, 32, 33, 48). Image data were stored as MATLAB data structure with an option to export as one of several standard compressed and noncompressed image formats. The MATLAB data structure used by KAMS preserved the 12-bit resolution of the camera for subsequent analysis. The data structure was indexed by channel, z-stack, time, field, and sample well (cztfw). In our scheme these indices corresponded to the optical channel imaged (c), the z-depth of focus in a multiple z-stack set of images (z), a time index for the purposes of long term time-lapse (t), the selected image field for a particular sample (f), and an index for the specific sample (w).

Automated Image Analysis. Mutants were analyzed using a custom image analysis program KAMS-analyze. The program was designed to reduce the image data to a numeric data set representing the biologically relevant parameters of all of the cells in the image fields. The output from the program is a data structure that represents the entire data set, with each individual cell represented by about 100 parameters. The steps in the analysis were:

(*i*) The original 1MP phase contrast images were analyzed to determine all individual nonoverlapping cell locations.
(*ii*) The original phase contrast image and the corresponding fluorescent images of the same field were segmented into 300 × 300 pixel subimages centered on particular cell locations.
(*iii*) Each image was adjusted and masked to isolate the cell of interest and the cell-free local background.
(*iv*) The membrane boundary was determined using a piecewise continuous spline applied to the phase contrast image after the application of a binary threshold.
(*v*) Fluorescence signal quantification and characterization was done for all cells in all of the fluorescence channels:
  (*a*) To find and quantify localized fluorescent peaks, a region-finding algorithm was used on fluorescent images after binary thresholding. Region maxima were taken to be candidate localized signals and coordinates. The threshold was set to allow a 3 sigma separation between cytoplasmic signal levels and peak signal levels. The algorithm allows any number of localized signals to be found, so long as they are statistically significant and pass several criteria used to eliminate spurious pixel noise.
  (*b*) To determine dispersed cytoplasmic fluorescent signal levels, the maximum number of fluorescent regions

found in the cell interior was determined as the threshold level was taken from the maximum to zero. As the threshold is dropped, the number of regions found will increment by one as additional discrete peaks are encountered. When the dispersed signal level is reached, the number of found regions rises to a maximum and then drops to one as all regions coalesce to a single region at zero threshold. The threshold where the maximum number of regions was found was taken as a measure of the dispersed cytoplasmic contribution to the total signal and subtracted from the localized signal. An overall background signal, determined from the fluorescent background in the extracellular region was also subtracted from both the dispersed and localized signals.

To make the analysis more rigorous some parts of the analysis were performed on renormalized image data scaled between zero and one, where a baseline of zero was set to the value of the minimum intensity pixel and a normalized intensity of one was assigned to the brightest pixel. The scale factors were preserved and the image data were translated back into the original fluorescence units after analysis.

Detection of Protein Localization Networks. As described in the previous section, after KAMS-analysis, individual cell images have been characterized by a set of biologically relevant measurements. In the next analysis, stage the data from all observed cells from a particular mutant strain are combined into statistical averages. In our case, we were interested in knowing the localized protein abundance, dispersed protein abundance, total protein abundance, cell ensemble polarity (average, bi-, mono-, ecto-, and nonpolar fractions), as well as the cell shape information. After characterizing the statistical distributions using mean, median, and standard deviation, mutant strains were compared to unmutagenized strains that serve as wild-type controls and a z-score was calculated. The z-score was defined as the difference between the measurement and the control, in units of the of the control measurement width .The steps taken at this stage were:

(*i*) Wells flagged as out of focus in the run log were removed.

(*ii*) For the continuous variables the overall median was calculated for each fluorescent channel.

(*a*) By-run medians were calculated for each channel and run-to-run variations were detrended.

(*b*) mCherry and CFP channels were scaled to the YFP channel median to normalize the three fluorescent channels to a common scale.

(*c*) A z-score was calculated for each ensemble metric and compared to a wild-type mean calculated as:

$$Z_{wc} = (S_{wc} - \langle S^{control} \rangle)/\sigma^{control}$$

where,
$\sigma^{control}$ is the mean average deviation of the unmutagenized reporter strain localized signal.
$\langle S^{control} \rangle$ is the median value of the unmutagenized reporter strain localized signal.
S_{wc} is the localized or dispersed signal for sample well w and optical channel, c.
Z_{wc} is the z-score for the localized or dispersed signal for sample well w and optical channel, c

(*iii*) For the ensemble averages of the categorical polar fraction variables:

(*a*) The fraction of unmutagenized cells in a mixed (unsynchronized) population showing bipolarity, monopolarity, ectopic-polarity, or nonpolarity was measured. Deviations from the um-mutagenized polarity fractions form the basis of the z-score for the bipolar and monopolar metrics.

(*b*) A z-score was calculated for bipolar and monopolar fractions as:

$$Z_{wc}^{bipolar} = \left(N_{wc}^{bipolar} - N_{wc}^{total} P_c^{bipolar}\right) / \sqrt{N_{wc}^{total} P_c^{bipolar} \left(1 - P_c^{bipolar}\right)}$$

where,
$P_c^{bipolar}$ is the bipolar probability measured using the unmutagenized reporter strain for channel c.
N_{wc}^{total} is the total number of cells for sample well w and optical channel c.
$N_{wc}^{bipolar}$ is the measured number of bipolar cells for sample well w and optical channel c.
$Z_{wc}^{bipolar}$ is the z-score for the bipolar signal for sample well w and optical channel c.

Once z-scores were formed, the data from dissimilar measurements could be analyzed together. Hierarchical clustering was performed with the MATLAB (The MathWorks, Inc.) clustergram function (Bioinformatics Toolbox) and related subroutines. The localization phenotype of each mutant candidate was represented by a 12-dimensional vector composed of the calculated z-scores for each of the three fluorophores characterized by the L (localized), D (dispersed), B (bipolar), and M (monopolar) metric. To reduce the number of unreliable measurements due to possible systematic errors and sampling error, data derived from images with poor focus performance or with less than 10 cells were eliminated. Using Euclidean pair-wise distances and linkage based on the average distance between clusters, hierarchical clustering was performed along the genotype axis. We judged the purity (true positives/true positives + false positives) and efficiency (true positives/true positives + true negatives) of cluster identification by assessing the variation in our ability to isolate the numerous *podJ* disruptions into a single well-defined cluster. The number of mutants with *podJ* disruptions was stable with respect to the choice of the quality selection criteria over a wide range, as was the contamination of the podJ cluster with unmutagenized controls. Optimizing cluster purity and efficiency over this broad maximum led us to select data with the z-score variance greater than 0.7 and L and D-metric values with relative standard errors of the mean less than 0.5. These choices are somewhat arbitrary, but the specific choice did not have a strong effect on the membership of the four most significant clusters.

Network Ordering Using Epistatic Interaction Mapping. To determine the connectivity between identified genes involved in protein localization and further infer the underlying genetic network a set of epistasis experiments was performed. Low copy number plasmids bearing either *tacA* or *spmX* under control of the inducible promoters *Pxyl* or *Pvan* were introduced into a set of transposon insertion mutants belonging to cluster B, D, and a subset of cluster C. The localization pattern of each resulting strain was analyzed using KAMS (Tables S1, S2, and S3). In this way, the results of the complementation experiments could be compared directly and quantitatively to the data from the mutant library. Note that the data in Tables S1 and S2, although quantitative, is not absolute. Rather, the scale has been set by setting the amount of signal seen in the unmutagenized labeled control strain to 100% and measuring all other mutants relative to the control strain.

1. Viollier PH, Sternheim N, Shapiro L (2002) A dynamically localized histidine kinase controls the asymmetric distribution of polar pili proteins. *EMBO J* 21: 4420–4428.
2. Ohashi T, Galiacy SD, Briscoe G, Erickson HP (2007) An experimental study of GFP-based FRET, with application to intrinsically unstructured proteins. *Protein Sci* 16: 1429–1438.
3. Thanbichler M, Iniesta AA, Shapiro L (2007) A comprehensive set of plasmids for vanillate- and xylose-inducible gene expression in. *Caulobacter crescentus. Nucleic Acids Res* 35:e137.
4. Jacobs MA, et al. (2003) Comprehensive transposon mutant library of. *Pseudomonas aeruginosa. Proc Natl Acad Sci USA* 100:14339–14344.
5. Zhang Z, Schwartz S, Wagner L, Miller W (2000) A greedy algorithm for aligning DNA sequences. *J Comput Biol* 7:203–214.

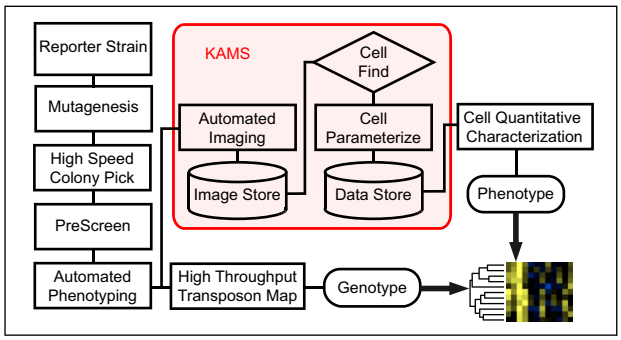

Fig. S1. Process flow. Major process steps are shown for the identification of protein localization networks using automated quantitative fluorescence microscopy. All steps in the processes were optimized for high throughput.

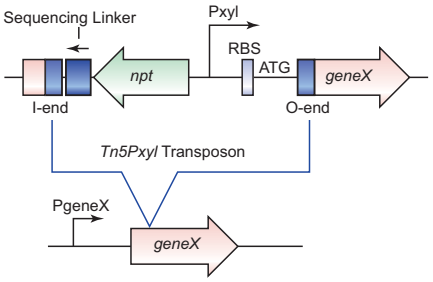

Fig. S2. Mutagenesis strategy using the *Tn5Pxyl* transposon element. The *Tn5* derivative *Tn5Pxyl* contains at one end, two nested primer binding sites (Sequencing Linker) used for insertion site mapping. At the other end, the *Tn5Pxyl* element contains an outward facing inducible promoter (Pxyl) and a ribosomal binding site (RBS) followed by a start codon (ATG). When inserted in the correct orientation upstream of a target gene, transcription from the native promoter (PgeneX) is abolished but can be conditionally reinitiated from the inducible Pxyl promoter upon addition of xylose. Alternatively, in frame insertion within the 5′ region of a target gene will enable conditional expression of the target gene (geneX).

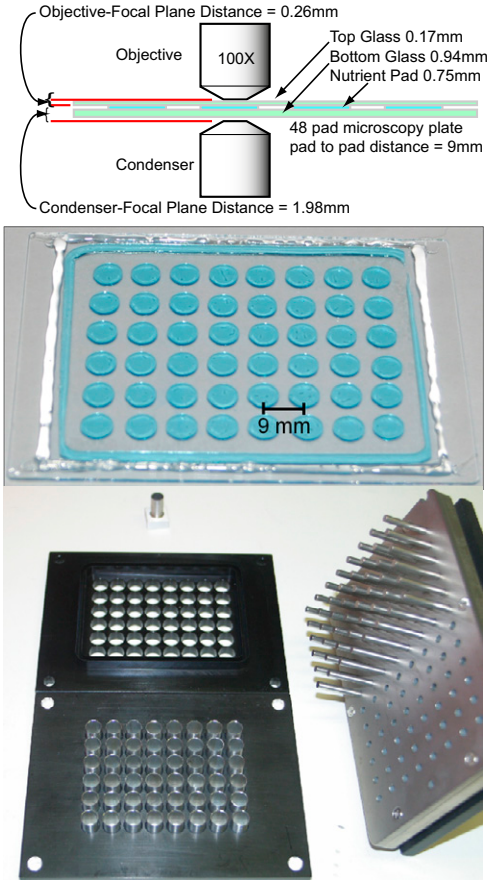

Fig. S3. Microscopy plate for 100× live cell fluorescence imaging. In the upper drawing the tolerances required for 100× imaging are shown along with a cross sectional view of the 48-well microscopy plate. Seen in the first image (*Middle*) is a view of the 48-well microscopy plate from above, showing the independent agarose pads and an agarose border used to stabilize the cover glass and provide a vapor seal. In the image, the top glass (cover glass) is in place and has been sealed to the bottom glass with thermoplastic glue from a hot glue gun. Pads have been artificially colored for visibility. The pads are cut from a 0.75 mm thick cast agarose sheet using the custom tooling shown in the lower image. Bacteria are stamped onto the plate from 96-well growth plates using a 48 floating flat pin tool (*Bottom Right*).

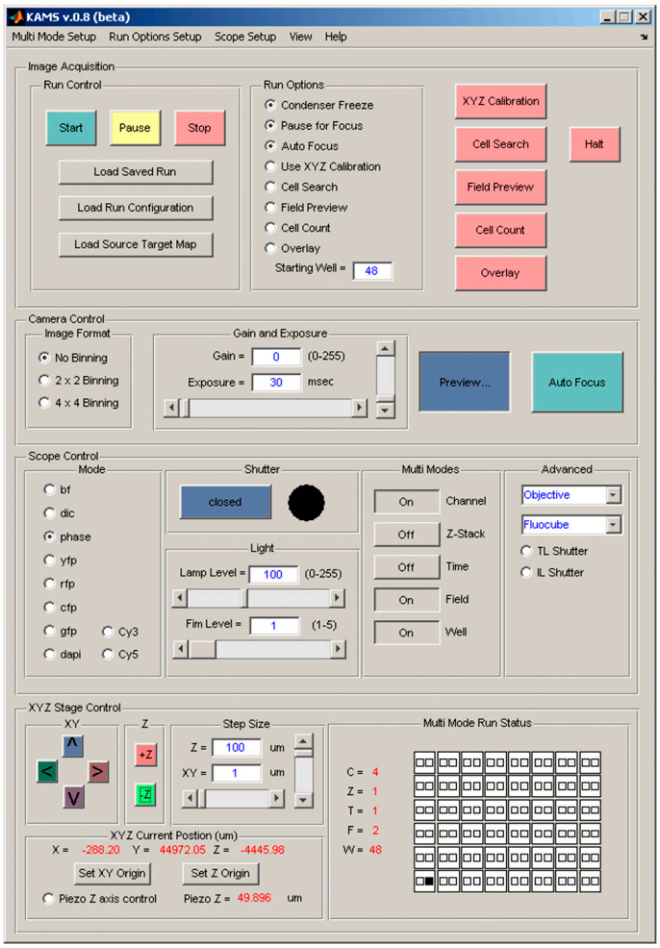

Fig. S4. KAMS screen shot. "KAMS–acquire" software user interface screenshot. Lowest panel controls XYZ stage motion and piezo electric focusing. Mid-lower level panel implements manual and automatic modes of scope control. Midupper level panel controls cooled CCD camera. Upper level panel controls automated image acquisition. In addition, setup menus control configuration of multiple mode running, run options and the microscope configuration.

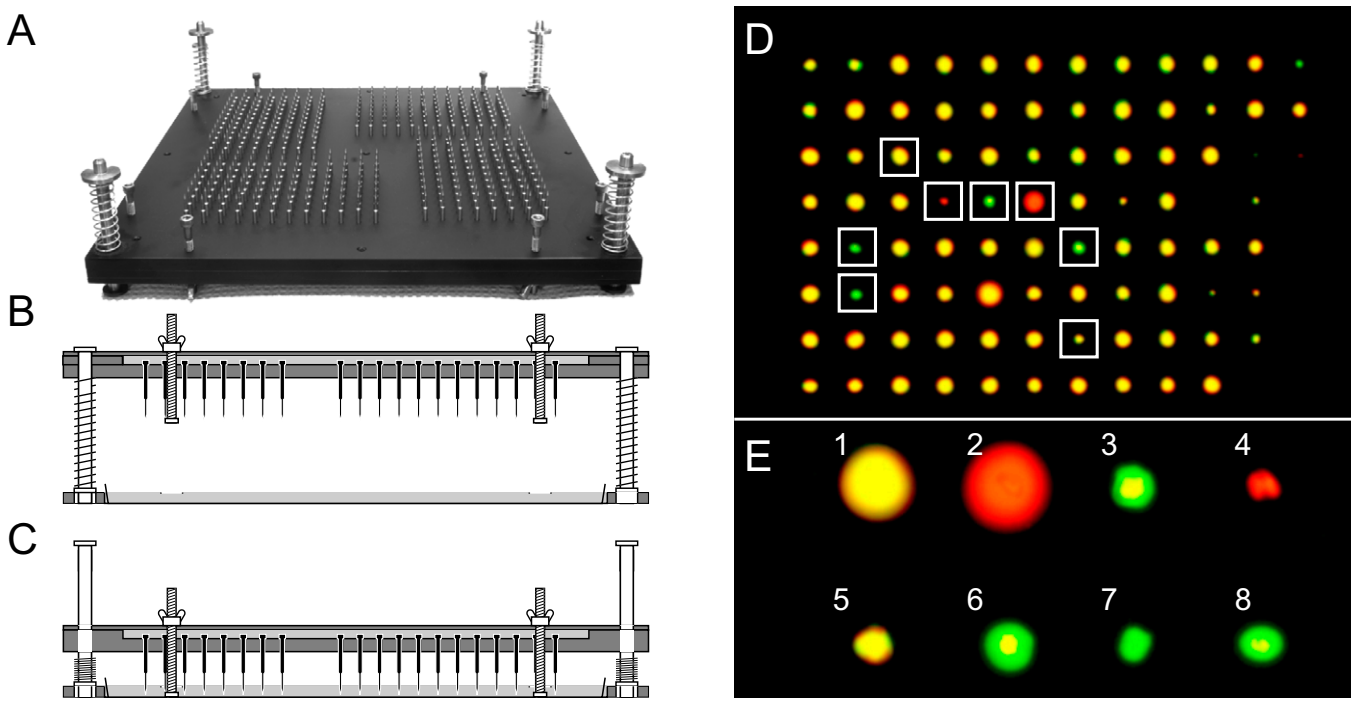

Fig. S5. Soft agar assay. The custom-designed precision 384 floating pin-tool used to transfer nanoliter samples from four 96-well growth plates onto assay trays containing PYE soft agar is shown. The precise positioning of the innoculum with the pin tool facilitated easy indexing and image registration during scanning and analysis of swarm size and differential growth rate. (*A*) An image of the pin plate is shown inverted. The registration (*Lower*) plate is not shown in the photo. (*B*) The neutral position is shown with the pin plate engaged with the registration plate above the soft agar growth tray. (*C*) The engaged position is shown, with the pins penetrating the soft agar to an adjustable depth. (*D*) A difference image calculated between swarmer assay plates containing and lacking inducer is shown in pseudocolors. Individual mutants with similar swarming phenotypes under both conditions are highlighted in yellow. Mutant candidates that exhibit a conditional swarming defect in presence or absence of the inducer xylose are shown in green and red. (*B*) Magnified images of representative mutants (white squares in *A*) exhibiting wild-type swarming behavior (*1*), nonconditional swarming defects (*5*), conditional growth (*4*, *7*) and conditional swarming defects (*2*, *3*, *6*, *8*) are shown.

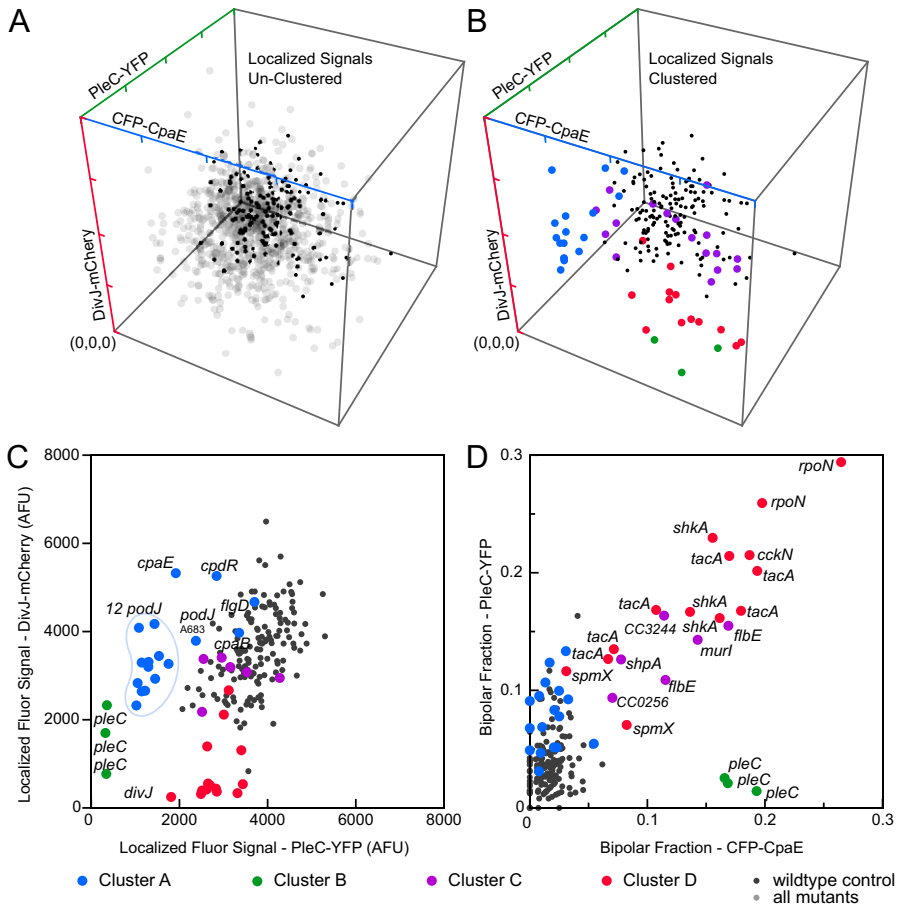

Fig. S6. Low dimensional view of localization phenotypes retrieved from the automated microscopy screen. (*A*) 3D view of the localized fluorescence signal values plotted for the unmutagenized control strain (black) and the set of all mapped transposon mutants (gray). (*B*) The same 3D view with only the unmutagenized control strain (black) and the set of all mapped transposon mutants that fall in to distinct clusters as determined by hierarchical clustering: cluster A (blue), cluster B (green), cluster C (purple), cluster D (red). (*C*) 2D projection onto the PleC-YFP, DivJ-mCherry plane of the signals shown in *B*. Gene disruptions belonging to clusters A, B, D, and the isolated *Tn5* insertion within *divJ* are labeled with allele names. Only a subset of cluster C is shown because it is not distinguished in this projection. Multiple hits within the *podJ* gene are highlighted (blue lasso) excluding the transposon insertion causing a frame shift at A_{683}, which is shown separately. (*D*) Bipolar PleC-YFP and CFP-CpaE fractions are plotted. Transposon mutants belonging to cluster B, D and a subset from cluster C (purple) are labeled with the corresponding allele names.

Table S1. Relative localized PleC-YFP signal within a set of pili gene deletions

Genotype: NA1000	Localized PleC-YFP signal	Total cellular PleC-YFP signal
pleC::yfp	100% ± 4.3%	100% ± 0.2%
pleC::yfp, ΔpilA	90% ± 6.7%	99% ± 0.1%
pleC::yfp, ΔcpaA	85% ± 5.6%	97% ± 0.3%
pleC::yfp, ΔcpaB	102% ± 1.5%	99% ± 0.1%
pleC::yfp, ΔcpaC	92% ± 4.6%	98% ± 0.2%
pleC::yfp, ΔcpaD	87% ± 3.7%	98% ± 0.1%
pleC::yfp, ΔcpaE	53% ± 4.4%	99% ± 0.3%
pleC::yfp, cpaF::Tn5	87% ± 3.5%	99% ± 0.2%
pleC::yfp ΔcpaE ; pBXMCS_6::cpaE	116% ± 6.3%	105% ± 0.2%

Values are mean ± SEM.

Table S2. Relative localized DivJ signal in different strain backgrounds

Genotype	No plasmid	pBVMCS_6::*tacA*	pBXMCS_6::*spmX*
wt reporter strain	100% ± 11.1%	148% ± 34.5%	101% ± 44%
pleC::TnPvan P379h1	11% ± 0.5%	74% ± 8.0%	82% ± 14%
tacA::TnPxyl P260a4	6% ± 0.4%	140% ± 7.3%	87% ± 7%
shpA::TnPvan P342h12	17% ± 7.8%	90% ± 17.8%	102% ± 36%
shkA::TnPvan P353h5	20% ± 5.1%	81% ±13.9%	84% ± 33%
rpoN::TnPvan P324h9	7% ± 0.2%	7% ± 1.1%	82% ± 4%
cckN::TnPxyl P252g8	91% ± 14.6%	103% ± 6.2%	42% ± 1%*
cckN::TnPxyl P252g8 + xyl	65% ± 0.4%	171% ± 2.7%	118% ± 6%*
spmX::TnPxyl P210f5	10% ± 4.8%	7% ± 0.0%	75% ± 3%

Values are mean ± SEM.

*Basal level expression of *spmX* from the pBVMCS_6::*spmX* plasmid was used for complementation.

Table S3. Epistasis analysis–fraction of cells with bipolar CpaE or bipolar PleC distribution

Genotype	No plasmid	pBVMCS_6::*tacA*	pBXMCS_6::*spmX*
Fraction of cells with bipolar CpaE distribution			
wt reporter strain	1% ± 0.8%	1% ± 0.9%	4% ± 0.3%
pleC::TnPvan P379h1	21% ± 9.1%	17% ± 3%	7% ± 5.3%
tacA::TnPxyl P260a4	20% ± 1.4%	1% ± 0.1%	3% ± 0.4%
shpA::TnPvan P342h12	18% ± 3.5%	6% ± 0.1%	1% ± 0.6%
shkA::TnPvan P353h5	13% ± 2.5%	2% ± 0.9%	1% ± 0.4%
rpoN::TnPvan P324h9	35% ± 1.5%	24% ± 1.3%	21% ± 3.1%
cckN::TnPxyl P252g8	2% ± 0.9%	1% ± 0.1%	9% ± 3% *
cckN::TnPxyl P252g8 + xyl	18% ± 2.9%	1% ± 0.2%	12% ± 3.1%*
spmX::TnPxyl P210f5	7% ± 2.1%	14% ± 2.4%	2% ± 2.5%
Fraction of cells with bipolar PleC distribution			
wt reporter strain	1% ± 0.8%	1% ± 0.9%	4% ± 0.3%
pleC::TnPvan P379h1	NA	NA	NA
tacA::TnPxyl P260a4	16% ± 4.8%	6% ± 1.2%	5% ± 2.8%
shpA::TnPvan P342h12	17% ± 0.6%	9% ± 2.1%	3% ± 2%
shkA::TnPvan P353h5	12% ± 3.7%	7% ± 1.2%	2% ± 2.2%
rpoN::TnPvan P324h9	31% ± 0.3%	24% ± 4.2%	23% ± 0.5%
cckN::TnPxyl P252g8	5% ± 0.8%	8% ± 2.3%	9% ± 5%*
cckN::TnPxyl P252g8 + xyl	20% ± 0.2%	4% ± 1.5%	14% ± 1.8%*
spmX::TnPxyl P210f5	6% ± 1.3%	14% ± 0.1%	3% ± 1.7%

NA, not applicable, *Tn5Pvan* insertion within *pleC* causes disruption of the *yfp* reporter fusion.

Values are mean ± SEM.

*Basal level expression of *spmX* from the pBVMCS_6::*spmX* plasmid was used for complementation.